Provided for non-commercial research and education use.
Not for reproduction, distribution or commercial use.

This article appeared in a journal published by Elsevier. The attached copy is furnished to the author for internal non-commercial research and education use, including for instruction at the authors institution and sharing with colleagues.

Other uses, including reproduction and distribution, or selling or licensing copies, or posting to personal, institutional or third party websites are prohibited.

In most cases authors are permitted to post their version of the article (e.g. in Word or Tex form) to their personal website or institutional repository. Authors requiring further information regarding Elsevier's archiving and manuscript policies are encouraged to visit:

http://www.elsevier.com/copyright

Author's personal copy

Thin Solid Films 518 (2010) 2897–2904

Contents lists available at ScienceDirect

Thin Solid Films

journal homepage: www.elsevier.com/locate/tsf

Thin film removal mechanisms in ns-laser processing of photovoltaic materials

J. Bovatsek [a,*], A. Tamhankar [a], R.S. Patel [a], N.M. Bulgakova [b], J. Bonse [c,1]

[a] Newport Corp., Spectra-Physics Lasers Division North America, 1335 Terra Bella Ave, Mountain View, CA 94043, USA
[b] Institute of Thermophysics SB RAS, Lavrentyev Ave. 1, 630090 Novosibirsk, Russia
[c] Newport Spectra-Physics GmbH, Ruhlsdorfer Strasse 95, D-14532 Stahnsdorf, Germany

ARTICLE INFO

Article history:
Received 29 June 2009
Received in revised form 23 September 2009
Accepted 20 October 2009
Available online 29 October 2009

Keywords:
Thin films
Photovoltaics
Solar cell
Laser scribing
Damage threshold
Laser–matter interaction
Silicon
Copper indium gallium diselenide

ABSTRACT

The removal of thin films widely used in photovoltaics (amorphous silicon, tin oxide, zinc oxide, aluminum, and molybdenum) is studied experimentally using multi-kHz Q-switched solid-state lasers at 532 nm and 1064 nm wavelengths. The processing ("scribing") is performed through the film-supporting glass plate at scribing speeds of the order of m/s. The dependence of the film removal threshold on the laser pulse duration (8 ns to 40 ns) is investigated and the results are complemented by a multi-layer thermal model used for numerical simulations of the laser-induced spatio-temporal temperature field within the samples. Possible film removal mechanisms are discussed upon consideration of optical, geometrical, thermal and mechanical properties of the layers.

© 2009 Elsevier B.V. All rights reserved.

1. Introduction

Recent years have seen tremendous growth in emerging market economies throughout the world. The resulting rapid increase in resource consumption has driven the cost of energy to unprecedented levels. Accompanying this increased cost was increased interest in alternative energy sources such as photovoltaic ("PV") devices. And with every surge in the price of oil or gas, there was a corresponding surge in the financial viability of such alternatives. While recently the rate of global economic growth has waned, and the cost of energy has retreated accordingly, interest in solar cell technology remains strong. This is providing a source of continued demand for various support industries such as laser and laser-based system manufacturing.

The role of lasers in solar cell device fabrication continues to expand, with processes such as cutting, drilling, scribing, sintering, and annealing all being explored. For the highly-efficient crystalline silicon-based devices ("*c*-Si"), lasers are most commonly used for edge isolation scribing; but there is also a fast-growing application space with the increased fabrication of more exotic solar cells, such as "emitter wrap through" (via drilling) [1,2] and buried contact (scribing) devices [2,3].

An increasingly popular alternative to *c*-Si solar cells is thin film photovoltaic (TFPV) device technology, for which the most important laser process is laser thin film removal ("laser scribing" [4]) for electrical isolation of the individual segments of a monolithically integrated serial connection of solar cells [5]. This process involves the irradiation of a glass panel with a tightly-focused laser beam, thus resulting in the removal of one or more layers of thin film from either another thin film material, or from the glass panel itself. In the production of a thin film solar cell device, three scribe processes are typically performed (commonly referred to as the P1, P2, and P3 scribes), with various film deposition processes occurring in between. The P1 scribe removes a first electrical contact film from the glass substrate; the P2 scribe removes the solar absorber film from this first contact film; and the P3 scribe removes both the PV layer and a second electrical contact film from the first contact film [6]. For several years, this TFPV process technology has expanded in industry [7], and is now used routinely with nanosecond laser sources. Modern diode-pumped solid state ns lasers provide an excellent cost/performance ratio which allows, along with the reduced materials consumption, the reduction of the production costs of TFPV solar cells and large area solar modules.

This study focuses on laser thin film scribe processes for various thin film solar technologies including amorphous Silicon ("*a*-Si"; P1, P2, P3 scribes), Cadmium Sulfide/Cadmium Telluride ("CdS/CdTe"; P1 scribe only) and Copper Indium Gallium di-Selenide ("CIGS"; P1 scribe only). The energy density (also known as fluence) threshold for removal of the thin film(s) of interest is determined for various

* Corresponding author. Tel.: +1 650 966 5735; fax: +1 650 961 7101.
E-mail addresses: jim.bovatsek@spectra-physics.com (J. Bovatsek), joern.bonse@bam.de (J. Bonse).
[1] Present address: BAM Bundesanstalt für Materialforschung und -prüfung, Unter den Eichen 87, D-12205 Berlin, Germany.

0040-6090/$ – see front matter © 2009 Elsevier B.V. All rights reserved.
doi:10.1016/j.tsf.2009.10.135

Author's personal copy

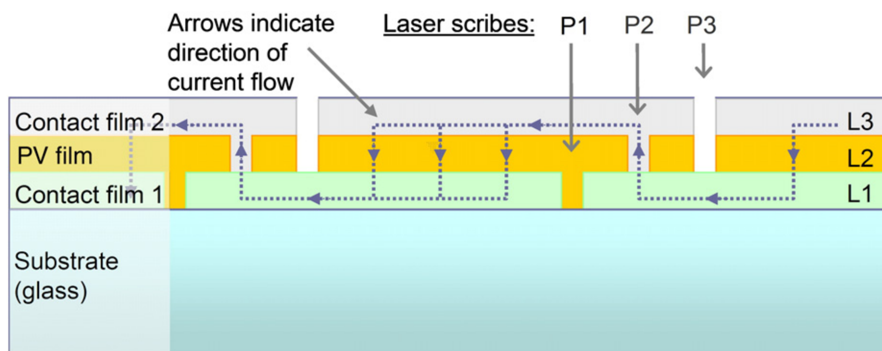

Fig. 1. Schematic showing the basic geometry and functioning of a thin film solar cell.

pulse durations (τ) between approximately 8 and 40 ns, and for IR (1064 nm) and green (532 nm) wavelengths. For selected scribe processes, experimental results are compared to those generated by a thermal model of the laser irradiation process.

1.1. Thin film photovoltaic devices

The monolithic thin film solar cell is increasingly the architecture of choice for solar cell manufacturing companies worldwide. There are several reasons for this, including attractive manufacturing scalability, opportunities for leveraging existing flat panel display technology, and the potential shortage of bulk silicon used for more efficient crystalline silicon solar cells. In addition, various process- and materials-related technology advancements are improving device efficiencies, resulting in an increasingly attractive balance between manufacturing cost and product performance [7,8].

Varieties of thin film solar cells include *a*-Si, CdS/CdTe, and CIGS; substrates for cell fabrication include several-millimeter thick soda lime glass as well as polymers and metals with thicknesses in the range of 10's of microns.

While the materials involved are varied, each with particular advantages and disadvantages, all thin film solar cells share the same basic geometry and working principle. Fig. 1 shows a cross-sectional schematic of such a typical thin film photovoltaic device. The materials are arranged in a layered system such that there are two electrically-conducting "contact" surfaces ["front-side" (facing the sun) and "back-side" contacts] with a semiconductor (PV) material as solar absorber in between. Front-side electrical contacts utilize transparent conducting oxide materials, such as indium doped tin oxide or SnO_2, which allow both sunlight and electricity to propagate within them with minimal loss.

The laser scribes are identified as "P1", "P2", and "P3" and their purpose is to divide the large, meter-sized solar panels into several narrow PV cells operating electrically in series. This results in a more practical and efficient low-current/high-voltage device.

1.2. Thin film scribing with Q-switched ns lasers

Various types of lasers are employed for thin film scribing, with diode-pumped solid state Q-switched lasers, at both infrared and green wavelengths, among the most common. Short pulse widths in the range of 10's of nanoseconds combined with 10's of microJoule pulse energy levels provide sufficient intensity for most film removal tasks. To meet the throughput demands of high-volume manufacturing, relative motion between the glass panel and the irradiating laser beam (achieved either by beam scanning, or panel motion) is minimally several hundred mm/s, and up to several m/s in the most advanced systems. To keep up with the high-speed motion, the lasers must be capable of generation pulses at a rate of 10's to 100's of kHz.

When possible, it is generally preferred to scribe with the laser incident from the substrate-side of the target film(s). For example, if the goal is to remove an absorbing metal film from a transparent glass substrate, the laser pulses will ideally travel through the glass before irradiating the metal/glass interface. Fig. 2 illustrates such a scenario, and indicates the various physical phenomena (ablation, delamination, etc.) that are potential contributors to the film removal process.

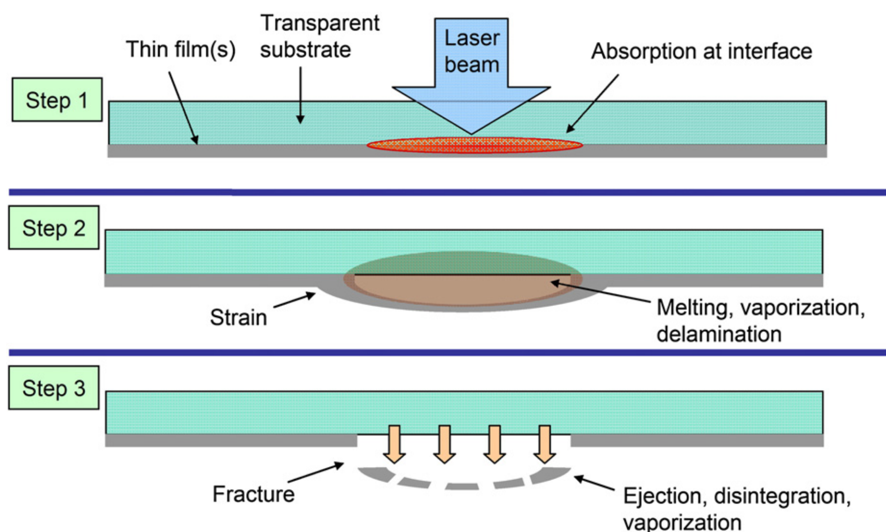

Fig. 2. Illustration depicting thin film removal with laser incidence through the transparent substrate.

Author's personal copy

Generally, the thin film removal process with ns-pulse irradiation may be considered to occur in three steps (Fig. 2). During the first step, the optical laser pulse energy is absorbed at the film/glass interface leading to steep temperature increase. During the second step, this temperature increase leads to local thermal strain and eventually to melting and evaporation. If fracture or sufficient evaporation occurs, the film may disintegrate and ablate in the subsequent third process step.

Compared to film-side irradiation, this method can lead to more efficient scribing through a reduction in fluence threshold for laser damage and/or the ability to remove the entire film with single- vs. multi-pulse processing. Additional potential benefits include less debris formation/deposition, and less plasma/debris shielding of the laser pulses. Care must be taken to avoid excessive absorption by the substrate of the irradiating light, leading to substrate damage; however for the common case of a (transparent) glass substrate and IR or green laser wavelength, this is generally not a concern since the threshold for film removal is typically lower than that for damaging the glass.

2. Experimental details

In this study, four different laser systems were used to execute four unique scribe processes, including two P1 scribes and the *a*-Si P2 and P3 scribes. For each of the processes, film removal thresholds were determined for 532 nm irradiation wavelength at three unique pulse durations between about ~8 ns and 40 ns (full width at half maximum). In addition, P1 scribe thresholds were determined for 1064 nm irradiation wavelength and sub-10 ns pulses. The scribed thin film materials include molybdenum, SnO_2, *a*-Si, and a film stack composed of *a*-Si/ZnO/Al. The base substrate material for all film stacks is ~3 mm thick soda lime glass; however the *a*-Si and *a*-Si/ZnO/Al layers are deposited on top of a SnO_2 film (which is ideally undamaged by the laser scribe process). Scribe threshold values were determined by correlating variations in applied pulse energy with the size of the resulting film removal areas (see Section 2.3).

2.1. Laser systems

Four different Newport/Spectra-Physics diode pumped solid state Q-switched laser systems were used to generate data presented here: Explorer™ 532 nm and 1064 nm system, BL6S™ 532 nm laser system, and Navigator II 532 nm laser system. A listing of the operating parameters for the lasers can be found in Table 1. In combination, this group of lasers is capable of generating a range of average power levels (~1–10 W) and pulse durations (~6–70 ns), with the capability of both infrared (1064 nm) and green (532 nm) output wavelengths. Furthermore, the four systems all have TEM00 mode output with a beam quality of $M^2<1.3$. For the threshold tests, the lasers were used to generate pulse durations in the range of 8 ns (Explorer™) to 37 ns (Navigator II).

In Table 1, the quoted power levels are typical maximum. For the BL6S™ and Navigator II laser systems, the output power at 532 nm changes significantly with the pulse repetition frequency (PRF) because the harmonic conversion efficiency changes with changes in pulse energy (high PRF = low pulse energy, and vice-versa). Conversely, the Explorer™ 532 nm laser system uses intra-cavity harmonic conversion, which allows for a more constant output power through a wide range of repetition rates. Also note that the pulse durations are specified as a range of values. Larger values are achieved by operating the laser at a higher PRF, and smaller values are achieved with lower PRF.

Table 1
Performance specifications of lasers used in the tests.

Laser system	Wavelength [nm]	Av. power [W]	PRF, range [kHz]	Pulse width [ns]
Explorer™-532	532	>1	20–150	~6–18
Explorer™-1064	1064	>1.75	20–150	~6–18
BL6S-532	532	>2.7	10–60	~7–14
Navigator™ II	532	>9	15–100	35–70

2.2. Optical setup

The optical setup used for the tests consists of four steering mirrors directing the laser pulses into a galvanometer-based beam scanning system ("galvo scanner", ScanLab, HurryScan II) with 10 mm diameter input aperture. Two different f-theta lenses with focal lengths of 80 mm and 160 mm were used for all beam focusing. When necessary, beam-collimating and/or beam-expanding optics were implemented to help in generating the desired optical spot sizes. All threshold data were generated with focused $1/e^2$-beam diameters in the range of 30–55 µm (verified experimentally). The laser pulse energies were determined from the average power (P) of the laser beam in the sample plane (as measured with a thermopile detector) along with the chosen pulse repetition frequency.

2.3. Threshold determination

When discussing a material's "damage" or "ablation" threshold, it is important to clarify precisely what phenomenon the threshold is for. In many cases, a laser damage threshold is simply the energy density (in J/cm^2) which causes a visible surface modification of the material; alternatively, the threshold of interest may be that fluence which results in crater formation in the material. For identical materials, we would likely find a large discrepancy in threshold values for (i) slight visible surface modification and (ii) measureable removal of bulk material.

In the case of laser thin film photovoltaic scribing, we are interested in *complete removal of the film* to the extent that is detectable with optical microscopy and/or surface profilometry (in practice, the true success of a PV scribe is defined by the final photo-electrical performance of the finished solar cell; however, experience has shown that visual inspection is usually a sufficient predictor of performance). Hence, the thresholds presented here represent the fluence that will result in the complete removal of the particular film(s) of interest from the immediate underlying material (substrate).

One very straightforward method to determine the threshold fluence for laser-induced bulk material modification has been described first in 1982 by J.M. Liu [9], and has been later adopted for application to thin film removal by several other researchers [10–12]. The method involves generating single-pulse laser damage features at different pulse energies (but the same focus spot size), measuring the diameters of the features, and using log-linear regression analysis to infer the relevant threshold fluence. This technique is attractive because in addition to the threshold information, it also allows for precise experimental determination of the optical spot size that was used to generate the features. This value can then be compared to a calculated value based on Gaussian beam propagation theory to further validate the threshold results. All fluence values referred to in this work are peak fluences of a spatially Gaussian beam distribution (with a $1/e^2$-decay radius w_0) incident at the air interface of the glass substrates on which the films reside. We estimate the absolute accuracy of the thresholds derived with this method at ±20%.

3. Results and discussion

Removal thresholds were determined for single-layer thin films of SnO_2 (*a*-Si and CdS/CdTe devices, P1 scribe), molybdenum (CIGS device, P1 scribe), amorphous silicon (*a*-Si device, P2 scribe), and a multilayer stack of *a*-Si + ZnO + aluminum (*a*-Si device, P3 scribe).

Author's personal copy

Table 2
Film removal thresholds for different materials, pulse durations and wavelengths.

Scribe type	TFPV type	Film(s)/substrate	Film/substrate thickness [μm]	Wavelength [nm]	Pulse width [ns]	Optical spot size, $1/e^2$ [μm]	Fluence threshold [J/cm^2]
P1	*a*-Si, CdS/CdTe	SnO_2/glass	0.650/3000	532	9	33	1.43
				532	13	43	1.03
				532	37	38	2.04
P1	*a*-Si, CdS/CdTe	SnO_2/glass	0.650/3000	1064	7	44	2.19
P1	CIGS	Mo/glass	0.293/3000	532	9	36	1.22
				532	13	54	1.21
				532	37	37	1.07
P1	CIGS	Mo/glass	0.293/3000	1064	7	39	1.01
P2	*a*-Si	*a*-Si/SnO_2	0.220/0.675	532	7	50	0.165
				532	13	51	0.115
				532	17	32	0.182
				532	37	40	0.194
P3	*a*-Si	Al + ZnO + *a*-Si/SnO_2	0.570/0.660	532	13	51	0.110
				532	17	33	0.181
				532	37	43	0.247

These materials are used extensively in the thin film photovoltaic industry; and scribe processes involving them are required in the manufacture of various TFPV devices. The removal threshold values determined for the various pulse durations, wavelengths, and scribe processes are listed in Table 2 along with relevant experimental parameters (film thicknesses, etc.). For SnO_2 and molybdenum, the threshold is for complete film removal from a glass substrate; for the *a*-Si P2 and P3 scribes, the threshold is for complete removal from a sub-micron thick layer of SnO_2 film on glass. The data show a wide range of removal thresholds among the various materials, from ~0.1 to >2.0 J/cm^2 (20:1 variation in fluence). In addition to the threshold values, the table also shows the approximate $1/e^2$-spot size (diameter) in the sample plane that was extracted from the threshold-determination data.

With knowledge of the film removal thresholds, it is then possible to optimize the laser parameters and generate continuous scribes of removed material, exactly as required in the manufacture of the solar cell devices. Fig. 3 shows optical microscope photos (bright field) of such scribes for the materials that were studied, using the focused beam sizes listed in Table 2. These data demonstrate that the chosen laser sources are suitable for thin-film solar cell production at scan speeds on the order of m/s, even at relatively low power levels (i.e. <1 W).

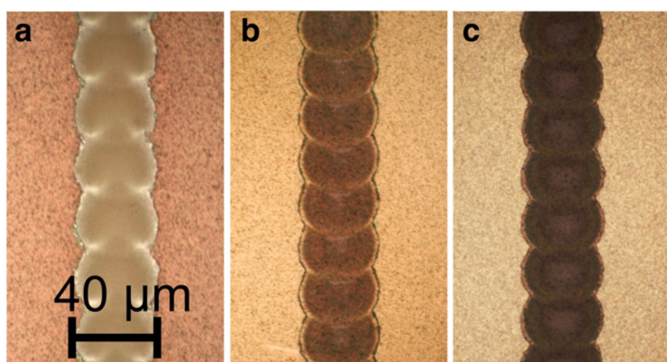

Fig. 3. Bright field optical micrographs of P1, P2, and P3 *a*-Si thin film photovoltaic device scribes generated by an Explorer laser [13 ns pulse duration, 532 nm wavelength]. (a) P1 scribe in a 650 nm thick SnO_2 layer on glass [0.5 m/s, PRF = 20 kHz, *P* = 0.75 W]; (b) P2 scribe in a 220 nm thick *a*-Si layer on a SnO_2 film (675 nm) coated glass [1.4 m/s, PRF = 60 kHz, *P* = 0.33 W]; (c) P3 scribe in a 570 nm thick Al/ZnO/*a*-Si multi-layer on a SnO_2 film (660 nm) coated glass [1.5 m/s, PRF = 60 kHz, *P* = 0.35 W]; all scribes were performed through the glass substrate.

3.1. P1 and P2 laser scribe thresholds: SnO_2 and molybdenum

For the P1 materials, threshold-dependence on pulse duration is not very definitive, with film removal thresholds at increasing pulse widths trending somewhat higher for SnO_2, and somewhat lower for molybdenum (Table 2). Based solely on thermal diffusion arguments, we might expect that, for longer pulse durations, the threshold would increase in proportion to the square root of the pulse durations [13]. However, for the case of thin films with thicknesses similar or below the spatial thermal diffusion length during the laser pulse irradiation time, it is not very surprising to see a breakdown in this relationship.

3.2. P2 and P3 laser scribe thresholds: amorphous silicon (*a*-Si)

The *a*-Si P2 and P3 scribe threshold results are of particular interest. Very little energy density is required for complete removal of the film (Table 2). Clearly, the strong absorption of silicon at 532 nm is assisting the film removal process. There is also a significant pulse-width dependence compared to the P1 scribe results. For a pulse duration change from 13 ns to 37 ns (2.85×), there is a threshold change of 0.115 to 0.194 J/cm^2 (1.68×) for the P2 scribe and 0.110 to 0.247 J/cm^2 (2.25×) for the P3 scribes. This result, which is visualized in Fig. 4, indicates that a clear processing advantage exists with, for example, ~10 ns vs. ~40 ns pulse durations, potentially allowing for 50% percent improvement in processing efficiency.

In addition to the strong threshold dependence on pulse duration, the *a*-Si P2/P3 threshold results are also interesting for their very low absolute fluence levels, irrespective of the irradiating pulse width. At the 532 nm wavelength, the regime of 0.1–0.2 J/cm^2 for the complete

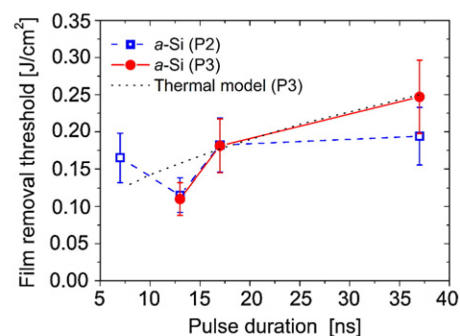

Fig. 4. Removal threshold fluence of the *a*-Si thin films (used in the P2 and P3 scribing process at 532 nm wavelength) vs. pulse duration.

Author's personal copy

removal of the *a*-Si films is significantly below damage threshold values reported for bulk crystalline silicon, where, at a comparable laser pulse duration of 18 ns, laser-induced melting has been observed for fluences larger than 0.35 J/cm^2 (see Ref. [14]). This cannot be explained solely by differences in the optical properties. Such a discrepancy indicates a different material removal mechanism and justifies a more detailed theoretical physical analysis.

3.3. Thermal modeling and analysis

For the *a*-Si P2 and P3 scribes, a thermal model for the pulsed irradiation of the samples was applied. The output of the numerical analysis is the one-dimensional temperature vs. time distribution in the various layers of the film stack. Thermal modeling was recently performed for films on a substrate (metal on metal [15], metal on glass [16,17], polymer on glass [18], and for silicon based solar cell modules [5]) irradiated with fs- and ns-laser pulses but such a spatio-temporal model has not yet been applied to the case of a multiple thin film photovoltaic layer stack (including the L2 and L3 layers, see Fig. 1). The multilayer structures of interest are presented schematically in Fig. 5 as "sample 1" and "sample 2".

Details of the thermal model are described in Ref. [19]. Here we explain only its main features. The time-dependent temperature distribution in the irradiated sample $T(t,x)$ is governed by the heat flow equation in a one-dimensional form:

$$(c_p\rho + L_m\delta(T-T_m))\frac{\partial T}{\partial t} = \frac{\partial}{\partial x}\lambda\frac{\partial T}{\partial x} + \sum(x,t). \quad (1)$$

Here, ρ is the mass density of the target material; c_p and λ are the specific heat capacity and the thermal conductivity of the target material, respectively. The term $\Sigma(x,t)$ represents the spatio-temporal source of the laser energy which will be defined below. The term $L_m\delta(T-T_m)$ (L_m is the latent heat of fusion) is introduced for a case of melting of the irradiated sample. This term allows following the dynamics of the liquid–solid interface whose temperature is assumed to be continuous and equal to T_m.

Note that in the formulation of Eq. (1) thermal vaporization is disregarded in view of relatively low laser fluences which are insufficient for heating of the considered materials above the melting threshold and, thus, to initiate thermal vaporization.

Eq. (1) is calculated for each layer of a particular structure (Fig. 5) while taking into account the physical properties of a material composing the layer (see Table 3). Initially, the sample is assumed to be at room temperature (300 K). The glass substrate (its parameters are marked in the following by the subscript "FS") is considered to be

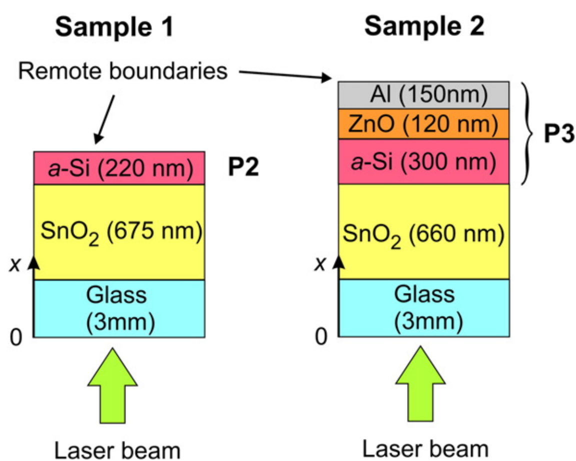

Fig. 5. Scheme of the two sample geometries ["sample 1" (left) and "sample 2" (right)] used in the thermal modeling analysis.

completely transparent and has the reflectivity R_{FS}. The laser pulse couples the SnO_2 layer from the side of the glass substrate so that the laser energy source in the SnO_2 layer (L1) is written as

$$\sum(x,t) = (1-R_{FS})(1-R_{L1})\alpha_{L1}I(t)\exp(-\alpha_{L1}(x-\Delta X_{FS})). \quad (2)$$

Here $I(t)$ is the incident laser pulse intensity with the Gaussian temporal shape (maximum intensity centered at $t=0$), α_{L1} and R_{L1} are the absorption and reflection coefficients of SnO_2 (note that the reflection coefficient is calculated taking into account that the light propagates through the boundary of two media with the values of dielectric permittivity ε_1 and ε_2), and x is the distance calculated from bottom of the calculational region (see Fig. 5). ΔX_{FS} is the thickness of the glass substrate, which is limited here to 2 µm (this was found to be sufficiently large for modeling of the heat penetration during the time of interest). For the absorbing *a*-Si layer (L2), the laser energy source is constructed in the following form:

$$\sum(x,t) = (1-R_{FS})(1-R_{L1})(1-R_{L2})\alpha_{L2}I(t)\exp(-\alpha_{L2}(x-\Delta X_{FS}-\Delta X_{L1})) \times \exp(-\alpha_{L1}\Delta X_{L1}), \quad (3)$$

where ΔX_{L1} is the thickness of the SnO_2 layer. The laser energy source terms are constructed similarly for the ZnO and Al layers of sample 2. However, it should be noted that, in view of relatively large thickness of the absorber, only a negligible portion of the laser energy reaches the ZnO and Al layers. The model provides also for the change in optical properties of L2 layer upon melting via reconstructing term (3) into molten and solid layers. However, for the irradiation regimes considered here, the melting temperature is not reached.

The boundary conditions at the interfaces between the layers provide for free heat flow that can be expressed in the following form

$$\lambda_{FS}\frac{\partial T}{\partial x}\Big|_{FS} = \lambda_{L1}\frac{\partial T}{\partial x}\Big|_{L1}, \lambda_{L1}\frac{\partial T}{\partial x}\Big|_{L1} = \lambda_{L2}\frac{\partial T}{\partial x}\Big|_{L2}, \text{etc.} \quad (4)$$

At the bottom boundary $x=0$ (Fig. 5), the temperature was considered to be 300 K and, at the upper remote boundary from the laser, the condition of the absence of heat flow through the surface was applied as $\frac{\partial T}{\partial x} = 0$. This condition implies the absence of vaporization in view of the relatively low applied laser fluences which, as will be demonstrated below, are too low to initiate melt and vaporization of the material. In the nanosecond time scale, we also disregard cooling of the surface by an ambient gas as well as radiative cooling.

The thermal problem (the differential equation including its boundary conditions) has been solved in only a one-dimensional approach, which is justified in view of the large irradiation spot size and comparatively shallow thermally-affected depth over the computational time. We have used an explicit numerical scheme with a spatial step of 2.5 nm and a time step of 20 ps which secure numerical scheme stability and good approximation of the solved differential equation.

Fig. 6 shows the results of the numerical integration of the thermal problem (Eqs. (1)–(4)) for ns-laser pulse irradiation (17 ns, 532 nm) of the two multi-layer systems of interest (sample 1 (Fig. 6(a)) and sample 2 (Fig. 6(b)) for the P2 and the P3 scribes, respectively) at the experimentally determined threshold value for complete *a*-Si film removal (0.18 J/cm^2). The spatio-temporal behavior indicates that the maximum temperature of ~1350 K is reached immediately after the laser pulse (the intensity maximum of the laser pulse is chosen at the time $t=0$), before heat diffusion along the layers redistributes the absorbed laser pulse energy and cools down the irradiated spot. Interestingly, the maximum temperature reached is very similar for both samples, which indicates that the additional Al/ZnO overlayers do not significantly affect the heat flow and the film removal thresholds. Moreover, the maximum temperature value of ~1350 K is below the melting (1420 K) and boiling (2654 K) temperatures of the (amorphous) silicon material [13]. This observation directly proofs that the thermal

Author's personal copy

Table 3
Material properties used in thermal modeling.

Parameter	Material	Value	Ref.
Density, ρ, [g/cm^3]	*a*-Si	2.2	[20]
	l-Si	2.52	[20]
	Glass	2.2	[20]
	Al	2.69	[21]
	SnO_2	6.95	[21]
	ZnO	5.7	[21]
Melting temperature, T_m, [K]	*a*-Si	1420	[13,20]
	Glass	1873	[13]
	Al	933	[21]
	SnO_2	1898	[21]
	ZnO	2248	[21]
Latent heat of fusion, L_m, [J/kg]	*a*-Si	1.32×10^6	[20]
	Al	4×10^5	[21]
	SnO_2	3.17×10^5	[21]
	ZnO	9.7×10^5	[13]
Specific heat, c_p, [J/(kg K)]	*c*-Si	$\begin{cases}184.36\times\exp(4.5\times10^{-3}T), & T<300\,K\\ 695.54\times\exp(2.375\times10^{-4}T), & T\geq300\,K\end{cases}$	[20]
	a-Si	C_p(*c*-Si)-8.0029 + 0.1017T	[20]
		800	[13]
	l-Si	910	[13,20]
	Glass	$708.11+0.29917\times T$	[20]
	Al	901	[21]
	SnO_2	353	[21]
	ZnO	494	[21]
Thermal conductivity, λ, [W/(m K)]	*a*-Si	1.8	[20]
	l-Si	$50.28+0.02933\times(T-T_m)$	[20]
	Glass	$\begin{cases}1.0056+1.3\times10^{-3}T, & T\leq1170\,K\\ 2.514, & T>1170\,K\end{cases}$	[20]
	Al	$\begin{cases}240, & T\leq400\,K\\ 240-0.05(T-400), & 400\,K<T<T_m\\ 93, & T\geq T_m\end{cases}$	[22]
	SnO_2	3.2	[13]
	ZnO	29	
Refractive index, $n+ik$ (at 532 nm wavelength)	*a*-Si	$4.49+i0.97$	[23]
	l-Si	$3.00+i4.80$	[24]
	Glass	1.50	[25]
	Al	$0.88+i6.48$	[23]
	SnO_2	$1.89+i0.01$	[26]
	ZnO	2.03	[27]

mechanisms of melting and subsequent evaporation are not responsible for the *a*-Si film removal when irradiating the sample with fluences near to the threshold fluence. Of course, when irradiating with a Gaussian intensity distribution, the fluence at the very center of the beam may be significantly higher than the (relatively low) threshold fluence that exists at the boundary of the region of removed film (for the case of a large single-pulse removal area).

The similarity of the maximum temperatures of ~1350 K reached upon irradiation of both samples suggests that the maximum temperature can be used in formulating a film removal threshold criterion. Due to the capabilities of our model, we have studied the pulse duration dependence of this criterion. In other words, for different pulse durations, the model was used to numerically calculate the fluence at which a maximum temperature of 1350 K is reached in the *a*-Si layer

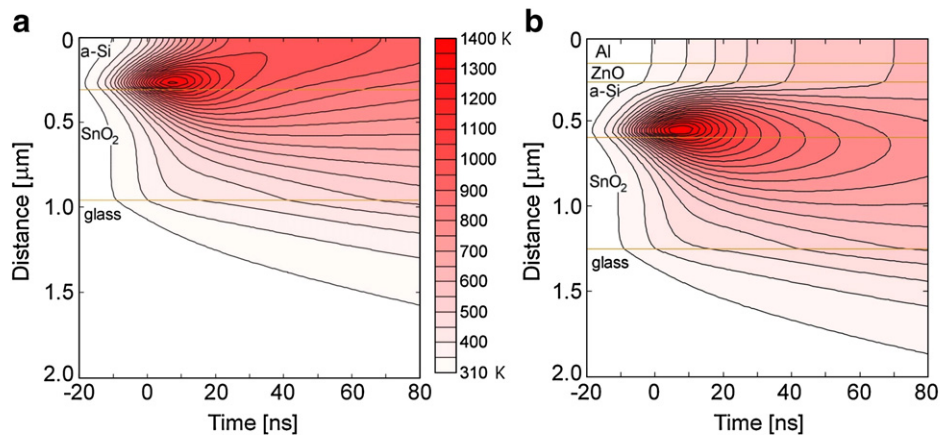

Fig. 6. Spatio-temporal behavior of the temperature in the *a*-Si P2 ((a), left, “sample 1”) and P3 ((b), right, “sample 2”) samples under irradiation of laser pulses (17 ns-laser pulse duration, 532 nm wavelength). The laser fluence of 0.18 J/cm^2 in both cases corresponds to the experimentally determined scribing threshold value. The maximum temperatures reached are 1360 K for sample 1 in (a) and 1335 K for sample 2 in (b), respectively. Note the common temperature scale and that distance here is counted from the remote boundary, contrary to the scheme shown in Fig. 5.

Author's personal copy

of sample 2. The results of these calculations are shown as dotted black line in Fig. 4. For the long pulse durations of 17 ns and 37 ns, an excellent agreement between the experimental data and the theoretical analysis is obtained, which justifies the assumptions made here. Only for short pulse durations (13 ns) some deviations can be observed, which its origin is not fully clear yet. An influence of the laser spot diameter can be excluded here, since (for a given laser system) a systematic variation of the optical beam spot size in the sample plane between 30 µm and 150 µm ($1/e^2$-diameter) did not result in a significant difference in the film removal threshold. Another possible origin might lie in difference in the longitudinal mode structure of the two different laser systems used in this study.

3.4. Thermal stress analysis

Since the threshold fluences of the *a*-Si P2/P3 scribes are found to be somewhat lower than what is required to initiate melting of the silicon, it is useful to further explore the problem. In particular, the effects of rapid thermal expansion due to fast heating via short-pulse laser irradiation should be considered.

To evaluate mechanical stress components generated in the *a*-Si film under fast heating, the approximate solution of the thermo-elasticity problem for a round plate with fixed edges may be used [16]:

$$\sigma_{r\,\max} = \sigma_{\theta\,\max} = \frac{E\alpha_l \Delta T}{2(1-\nu)}, \tag{5}$$

where E is the Young's modulus, α_l is the coefficient of linear thermal expansion, ν is the Poisson ratio, and ΔT is the temperature difference along the radius. For evaluation, we use the following mechanical properties of amorphous silicon: $E = 80$ GPa [28], $\nu = 0.22$ [28] and $\alpha_l \approx 4 \times 10^{-6}\,K^{-1}$ [29]. For the samples 1 and 2 at the experimentally determined threshold fluences (Fig. 4), the simulations have given the values ΔT in the range of 700–1000 K. This results in stress values within the *a*-Si layer in the range of 150–200 MPa. These values are much higher than the expected yield stress, which is below 10 MPa at $T \geq 700$ K for crystalline silicon [30]. The tensile strength, which is of order of a few GPas for single- and polycrystalline silicon [31,32] is much lower for amorphous silicon [32]. Hence, the irradiated area of the sample 1 experiences plastic deformations and can be fractured under laser-induced thermal stresses at temperatures well below the melting point. Additionally, a strong temperature gradient produced at the end of the laser pulse across the P2 layer (Fig. 6) facilitates expulsion of the film in the direction off the substrate, thus promoting its fracture.

With regard to the P3 scribe process (sample 2, Fig. 6(b)), the presence of the Al/ZnO layers atop the *a*-Si film may be considered to have two effects: (i) increased resistance to the fracturing of the *a*-Si layer, and (ii) partial heat extraction due to high thermal conductivity. However, note that the threshold laser fluence at 17 ns pulse duration is very similar for samples 1 and 2 (see Table 2). Furthermore, it is apparent that, while the Al/ZnO layer does in fact change the spatio-temporal temperature distribution within the *a*-Si film, it does not reduce considerably the maximum temperature reached in the layer. Hence, the rapid thermal expansion and associated thermal stress in the absorbing *a*-Si layer are similar for both samples.

Considering the mechanical aspects of the presence of the Al/ZnO films, we find that the tensile strength of ZnO films is reported to be quite high, on the order of 400 MPa [33] (for pure aluminum it is only 10–30 MPa [34]). We note, however, that tensile stress is usually reported for quasi-static loading. Dynamic loading of the nanosized Al/ZnO film on the nanosecond timescale, when the underlying heated silicon film expands abruptly, may in fact lead to failure of the brittle P3 film material, with the occurrence of crack formation and subsequent disintegration [35].

In discussing the mechanisms of film removal, there is a practical consideration – relating to the Gaussian intensity distribution of the irradiating laser beam – that should also be considered. When a single laser pulse removes a region of thin film, the outer periphery of this region demarcates where the irradiating energy density was precisely equal to the film removal threshold. Closer towards the center of the feature, the material is exposed to increasingly higher intensities. Depending on the pulse energy and beam focus spot size, this difference in fluence can be quite high; and in the context of P3 film removal, this central fluence may in fact be high enough to generate thermal strain beyond the tensile strength of ZnO. This would imply that there is a certain threshold fluence beyond which both the *a*-Si and the Al/ZnO films are removed; and below which the *a*-Si film is damaged, but the mechanical strength of the ZnO film prevents complete blow-off of the layers. This exact scenario was found within the data and is illustrated in Fig. 7, which contains microscope photos of features used to determine the film removal threshold for 532 nm wavelength and 13 ns pulse duration with optical beam spot size of 51 µm ($1/e^2$-diameter).

The photos in Fig. 7 indicate that the 1.71 µJ (0.167 J/cm^2) laser pulse energy is sufficient for generation of 22 µm wide features for both P2 and P3 film removal processes (Fig. 7(a) and (b)). However, the reduced pulse energy of 1.43 µJ (0.14 J/cm^2) is sufficient only for removal of the *a*-Si film [P2, Fig. 7(c)]. With the additional Al/ZnO film stack, the lower pulse energy results in only a bulging of the film, and a very slight fracture of the film at the center of the irradiation area, for the lower pulse energy [P3, Fig. 7(d)]. Note that in all cases (P2, P3), the local fluence at the feature boundary was 0.11 J/cm^2.

Finally, we would like to underline that the stress-related physical mechanism discussed here provides a very cost effective film removal method which is of enormous industrial relevance. In cases that the scribing quality has to be improved further, shorter laser wavelengths or shorter pulse durations in the fs- to ps-range might be used [12,17,36–39]. Such (more expensive) ps- or fs-laser pulses generally reduce the heat affected zone [12,38] around the laser scribes and, taking benefit from the high laser pulse peak intensity, allow to trigger non-linear energy deposition in the material [39,40].

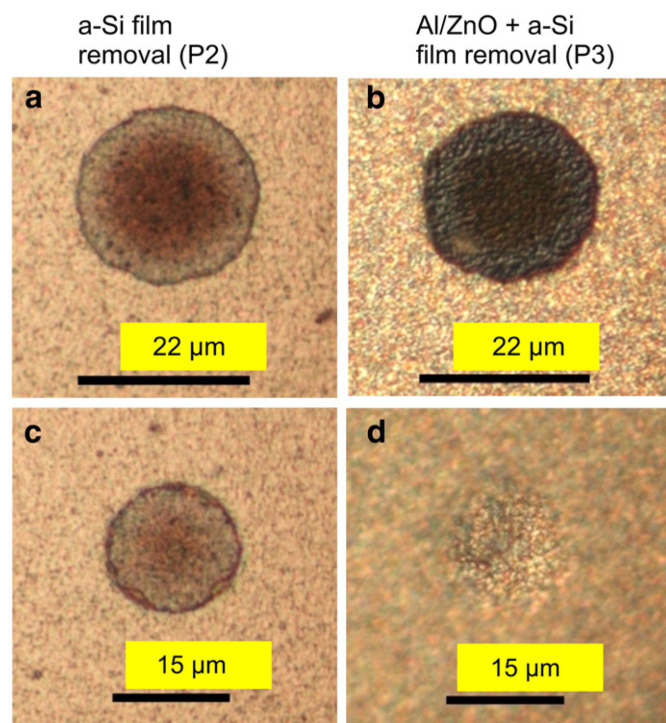

Fig. 7. Bright field optical micrographs of P2 and P3 film removal features using 532 nm, 13 ns-laser pulses [(a) and (b): 1.71 µJ; (c) and (d): 1.42 µJ]. For the lower pulse energy of 1.43 µJ, the mechanical strength of the ZnO film is sufficient to prevent complete film removal (picture at bottom-right).

Author's personal copy

4. Conclusions

Threshold-dependence on pulsed duration (8 ns–40 ns) for various thin film photovoltaic scribe processes (P1, P2, and P3) has been characterized, with selected scribes also being tested for wavelength dependence (1064 nm vs. 532 nm). For SnO_2 and molybdenum P1 scribing, there is no clear trending of film removal threshold with pulse duration; likewise, there is no clear advantage of using 532 nm over 1064 nm wavelength, or vice versa, in terms of the expected processing efficiency. However, threshold-dependence on pulse duration was clearly demonstrated for the *a*-Si P2 and P3 scribes (532 nm wavelength), with a noteworthy advantage for shorter pulses. Compared to 40 ns pulses, 10 ns pulses can process these films at ~50% lower energy densities, thus allowing for increased processing efficiency, reduced thermal loading of the substrate, and lower overall manufacturing costs for thin film photovoltaic devices.

For all pulse durations at the 532 nm wavelength, the film removal thresholds for *a*-Si P2 and P3 processes were found to be very low (0.1–0.25 J/cm^2). Thermal modeling of the pulsed irradiation process indicates that these fluence levels are too low to initiate melting of the silicon. However, additional thermo-mechanical analysis has shown that the thermal strain induced by rapid thermal expansion of the silicon is well beyond the material's yield strength, and is therefore likely responsible for fracture and delamination of the silicon (and additional layers atop it).

Our results demonstrate that, while no clear advantage exists for short pulse P1 scribe processes, there is a significant advantage for the *a*-Si P2 and P3 scribe processes. Within the range of pulse durations and wavelengths we have studied, execution of the three primary thin film photovoltaic scribe processes is easily achieved at the m/s level with the use of advanced Q-switched diode pumped solid-state lasers available in the market today.

Acknowledgement

The authors would like to thank Gonzalo Guadano for his efforts in supporting this work; his technical expertise is greatly appreciated.

References

[1] E. Van Kerschaver, G. Beaucarne, Prog. Photovolt. Res. Appl. 14 (2006) 107.
[2] N. Mingirulli, S. Trittler, M. Bui, A. Grohe, D. Biro, R. Preu, S. Glunz, 23rd European Photovoltaic Solar Energy Conference (23rd EPVSEC), Valencia, Spain, September 1–September 5, 2008, Conference Proceedings, 2008, p. 996.
[3] S.R. Wenham, B.O. Chan, C.B. Honsberg, M.A. Green, Prog. Photovolt. Res. Appl. 5 (1997) 131.
[4] A.D. Compaan, I. Matulionis, S. Nakade, Opt. Laser Eng. 34 (2000) 15.
[5] S. Nakano, T. Matsuoka, S. Kiyama, H. Kawata, N. Nakamura, Y. Nakashima, S. Tsuda, H. Nishiwaki, M. Ohnishi, I. Nagaoka, Y. Kuwano, Jpn. J. Appl. Phys. 25 (1986) 1936.
[6] S. Haas, A. Gordijn, H. Stiebig, Prog. Photovolt. Res. Appl. 16 (2008) 195.
[7] M.C. Gower, Opt. Express 7 (2000) 56.
[8] R. Patel, D. Clark, J. Bovatsek, 26th International Congress on Applications of Lasers & Electrooptics (ICALEO), Orlando, Florida, USA, October 29–November 1, 2007, Conference Proceedings, vol. 100, Laser Institute of America, 2007, (Paper 302).
[9] J.M. Liu, Opt. Lett. 7 (1982) 196.
[10] J. Jandeleit, G. Urbasch, H.D. Hoffmann, H.-G. Treusch, E.W. Kreutz, Appl. Phys. A 63 (1996) 117.
[11] J. Bonse, S. Baudach, W. Kautek, E. Welsch, J. Krüger, Thin Solid Films 408 (2002) 297.
[12] H.W. Choi, D.F. Farson, J. Bovatsek, A. Arai, D. Ashkenasi, Appl. Opt. 46 (2007) 5792.
[13] D. Bäuerle, Laser Processing and Chemistry, Third Edition, Springer-Verlag, Berlin, 2000.
[14] D.H. Lowndes, R.F. Wood, R.D. Westbrook, Appl. Phys. Lett. 43 (1983) 258.
[15] A. Melnikov, H. Prima-Garcia, M. Lisowski, T. Giessel, R. Weber, R. Schmidt, C. Gahl, N.M. Bulgakova, M. Weinelt, Phys. Rev. Lett. 100 (2008) 107202.
[16] Y.P. Meshcheryakov, N.M. Bulgakova, Appl. Phys. A 82 (2006) 363.
[17] J. Hermann, M. Benfarah, S. Bruneau, E. Axente, G. Coustillier, T. Itina, J.F. Guillemoles, P. Alloncle, J. Phys. D 39 (2006) 453.
[18] R. Fardel, M. Nagel, T. Lippert, F. Nuesch, A. Wokaun, B.S. Lukyanchuk, Appl. Phys. A 90 (2008) 661.
[19] N.M. Bulgakova, A.V. Bulgakov, L.P. Babich, Appl. Phys. A 79 (2004) 1323.
[20] S. De Unamuno, E. Fogarassy, Appl. Surf. Sci. 36 (1989) 1.
[21] I.S. Grigoryev, E.Z. Meilikhov, A.A. Radzig (Eds.), Handbook of Physical Quantities, CRC Press, 1995.
[22] Approximated on the basis of the temperature dependent data from G.V. Samsonov (Ed.), Physicochemical Properties of the Elements, Naukova Dumka, Kiev, 1965. (in Russian).
[23] E.D. Palik (Ed.), Handbook of Optical Constants of Solids, Academic Press, Orlando FL, 1998.
[24] M.S.K. Fuchs, J. Phys., Condens. Matter 12 (2000) 4341.
[25] I.H. Malitson, J. Opt. Soc. Am. 55 (1965) 1205.
[26] V.M. Jiménez, J.P. Espinos, A. Caballero, L. Contreras, A. Fernandez, A. Justo, A.R. Gonzalez-Elipe, Thin Solid Films 353 (1999) 113.
[27] K. Postava, H. Sueki, M. Aoyama, T. Yamaguchi, Ch. Ino, Y. Igasaki, M. Horie, J. Appl. Phys. 87 (2000) 7820.
[28] L.B. Freund, S. Suresh, Thin Film Materials, Cambridge University Press, 2003.
[29] J. Fabian, P.B. Allen, Phys. Rev. Lett. 79 (1997) 1885.
[30] J. Rabier, J.L. Demenet, Phys. Status Solidi (b) 222 (2000) 63.
[31] T. Tsuchiya, M. Hirata, N. Chiba, R. Udo, Y. Yoshitomi, T. Ando, K. Sato, K. Takashima, Y. Higo, Y. Saotome, H. Ogawa, K. Ozaki, J. Microelectromech. Syst. 14 (2005) 1178.
[32] T. Tsuchiya, 13th International Conference on Solid-state Sensors, Actuators, and Microsystems (Transducers '05), South Korea, June 5–June 9, 2005, Digest of Technical Papers, Part 2, 2005, p. 1953.
[33] C.W. Ong, D.G. Zong, M. Aravind, C.L. Choy, D.R. Lu, J. Mater. Res. 18 (2003) 2464.
[34] W. Martienssen, H. Warlimont (Eds.), Springer Handbook of Condensed Matter and Materials Data, Springer-Verlag, Berlin, 2005, p. 172.
[35] F. Zhou, J.-F. Molinari, Comput. Methods Appl. Mech. Eng. 194 (2005) 1693.
[36] D. Ruthe, K. Zimmer, T. Höche, Appl. Surf. Sci. 247 (2005) 447.
[37] S. Zoppel, H. Huber, G.A. Reider, Appl. Phys. A 89 (2007) 161.
[38] S. Küper, M. Stuke, Appl. Phys. B 44 (1987) 199.
[39] P. Rudolph, J. Bonse, J. Krüger, W. Kautek, Appl Phys. A 69 (Suppl.) (1999) S763.
[40] A. Mermillod-Blondin, J. Bonse, A. Rosenfeld, I.V. Hertel, Yu P. Meshcheryakov, N.M. Bulgakova, E. Audouard, R. Stoian, Appl. Phys. Lett. 94 (2009) 041911.